Endocrinology, 2022, **163**, 1–10
https://doi.org/10.1210/endocr/bqac157
Advance access publication 26 September 2022
Research Article

Loss of Anti-Müllerian Hormone Signaling in Mice Affects Trabecular Bone Mass in a Sex- and Age-Dependent Manner

Christiane van As,[1] Marijke Koedam,[1] Anke McLuskey,[1] Piet Kramer,[1] Najiba Lahlou,[2] Bram C. J. van der Eerden,[1,*] and Jenny A. Visser,[1,*]

[1]Department of Internal Medicine, Erasmus MC, Erasmus University Medical Center, P.O. Box 2040, 3000 CA, Rotterdam, The Netherlands
[2]Department of Hormone Biology and Metabolic Disorders, BPR-AS, 45700 Pannes, France

Correspondence: Jenny A. Visser, PhD, Department of Internal Medicine, Erasmus MC, Erasmus University Medical Center, P.O. Box 2040, 3000 CA, Rotterdam, The Netherlands. Email: j.visser@erasmusmc.nl.
*Both authors share last authorship.

Abstract

Ovariectomy-induced osteoporosis in mice results from an abrupt loss of ovarian sex steroids. Anti-Müllerian hormone knockout (AMHKO) mice show a gradual but accelerated ovarian aging, and therefore may better resemble osteoporosis following natural menopause. To study the impact of AMH signaling deficiency on bone, we compared trabecular and cortical bone parameters in 2-, 4-, 10-, and 16-month-old male and female wild-type (WT), AMHKO, and AMH type II receptor knockout (MRKI) mice using micro computed tomography (microCT). Goldner's staining was performed to confirm the observed bone phenotype. Both male and female AMHKO and MRKI mice showed age-dependent loss of trabecular bone ($P < 0.001$). However, reproductive-aged female AMHKO and MRKI mice had higher BV/TV compared with WT ($P < 0.001$), coinciding with increased growing follicle numbers ($P < 0.05$) and increased estrus inhibin B levels (AMHKO: $P < 0.001$; MRKI: $P < 0.05$) but normal inhibin A, estrogen, and progesterone levels. In aged female AMHKO and MRKI mice BV/TV did not differ from WT mice due to greater trabecular bone loss between 10 and 16 months compared with WT mice. At these ages, AMHKO and MRKI mice had reduced growing follicle numbers ($P < 0.05$) and reduced inhibin B levels ($P < 0.001$). At age 10 months, female MRKI mice had increased cortical bone parameters compared with WT mice ($P < 0.01$). Bone parameters of male AMHKO and MRKI mice did not differ from male WT mice. In conclusion, AMH signaling deficiency results in a sex- and age-dependent effect on predominantly trabecular bone. Our results further suggest that reproductive hormones beyond estrogen may contribute to bone homeostasis.

Key Words: AMH, AMHR2, bone homeostasis

Abbreviations: AMH, anti-Müllerian hormone (aka MIS); AMHKO, anti-Müllerian hormone knockout; AMHR2, AMH type II receptor; BV/TV, bone volume fraction; E2, 17β-estradiol; ELISA, enzyme-linked immunosorbent assay; FSH, follicle-stimulating hormone; microCT, micro computed tomography; MRKI, AMHR2 knockout (MIS receptor knockin); OVX, ovariectomized; ROI, region of interest; VCD, 4-vinylcyclohexene diepoxide.

Osteoporosis is characterized by reduced bone mass and worsening of the bone microarchitecture. This leads to increased bone fragility and fracture risk, especially in the hip, vertebrae, and wrist (1). Osteoporosis is a well-known disease of the elderly, and especially postmenopausal women are at risk to develop osteoporosis (2, 3). Indeed, the estimated lifetime risk of sustaining a fracture is 39.7% in Caucasian women and only 13.1% in Caucasian men at the age of 50 years, and above 50 years of age the fracture incidence in women is almost twice as high as in men (3, 4). Although bone loss occurs gradually throughout life in both men and women, women experience accelerated bone loss during the menopausal transition period (5, 6). The decline in estrogen levels is considered a major driver of postmenopausal osteoporosis (7).

In bone metabolism, estrogen stimulates bone formation and inhibits bone resorption. Loss of estrogens disrupts this balance, leading to increased bone turnover due to accelerated bone resorption by osteoclasts and diminished bone formation by osteoblasts. In cortical bone, the increased endocortical resorption combined with reduced periosteal apposition results in cortical thinning and increased cortical porosity. In trabecular bone, the increased bone resorption results in loss of trabecular connectivity (8-11).

Ovariectomy (OVX) of rodents to induce estrogen deficiency is a common model to study osteoporosis (12). In mice, OVX results in reduced cortical thickness, increased porosity, and loss of trabecular bone, thus showing features resembling postmenopausal osteoporosis (13, 14). Furthermore, OVX-induced osteoporosis in mice provides the possibility to apply this method in genetic mouse models. However, OVX results in an abrupt loss of ovarian sex steroids and growth factors, whereas during natural menopause in women this occurs more gradually (15). Furthermore, postmenopausal ovaries still produce androgens (16, 17). Therefore, a model that shows a more gradual decline in ovarian function might limit these drawbacks.

In women, natural menopause results from exhaustion of the primordial follicle pool. From this resting pool, follicles

Received: 28 February 2022. **Editorial Decision:** 21 September 2022. **Corrected and Typeset:** 18 October 2022

are continuously recruited to grow, from which ultimately per cycle only one follicle will ovulate in women and several in female mice. This process continues throughout reproductive life until the number of follicles has become too low to support menstrual cyclicity in women and menopause ensues. The decline in follicle number is paralleled by a decline in estrogen levels and loss of negative feedback on gonadotropins (15, 18). Ovarian aging in mice also shows this decline in follicle number and mice become anovulatory (19). We have previously shown that anti-Müllerian hormone knockout (AMHKO) mice display gradual but accelerated ovarian aging. AMH, also known as Müllerian inhibiting substance (MIS), is a member of the transforming growth factor β family and known for its role in Müllerian duct regression in male fetuses. It signals through a complex of a sole AMH type II receptor (AMHR2) with shared BMP type I receptors and male AMHR2 deficient mice are a phenocopy of male AMH-deficient mice (20, 21). In the ovary, AMH is expressed by the granulosa cells of preantral and small antral follicles and acts as a gatekeeper of follicle growth (22). In the absence of AMH, more primordial follicles are recruited, leading to a larger growing follicle pool at early reproductive age. Despite this increased recruitment, the number of ovulatory follicles is not different between AMHKO and wild-type mice. But as a consequence, the size of both the primordial follicle and growing follicle pool is exhausted at a younger age compared with wild-type mice (23). Since ovarian aging in AMHKO mice occurs at an earlier age than in wild-type mice but still gradual, in contrast to OVX mice, female AMHKO mice may serve as a suitable mouse model for osteoporosis following natural menopause. To study the impact of this accelerated ovarian aging on bone, we have analyzed various bone parameters in female AMH and AMHR2 deficient mice at various ages. We also included male mice deficient in AMH signaling in our studies.

Material and Methods

Mice

Wild-type (WT), AMHKO, and AMHR2 knockout (MRKI) mice were generated as described previously (20, 21, 23). The MRKI mice (MIS receptor knockin, in which 4.4 kb of the receptor locus that includes the first 6 exons is replaced with a LacZ cassette) were kindly provided by Dr. R. Behringer. AMHKO and MRKI mice and WT littermates on a C57Bl/6 background were housed at standard animal housing conditions at the Animal Facility of the Erasmus MC, which operates in compliance with the "Animal Welfare Act" of the Dutch government. The experiments were performed with permission of the local ethics committee. Mice were sacrificed at 2, 4, 10, and 16 months of age (n = 8-12 mice per genotype and sex) as described previously (24). For steroid hormone measurements, 4-month-old female mice were sacrificed on each day of the ovarian cycle (n = 5 per cycle day). Daily vaginal smears were taken for a period of at least 2 weeks as described previously to determine the day of the cycle (23). Cycle length and regularity was determined by analyzing 2 complete cycles.

Body weight and weight of testes and ovaries were determined. Femurs were collected and a blood sample was taken. The left testis and left ovary were fixed in Bouin's fixative. The left femurs were fixed in 10% formalin for 48 hours followed by preservation in 70% ethanol.

Follicle Counting

The number of growing follicles was determined as described previously (n = 5 mice per genotype) (24), using 8-µm sections, mounted on glass slides and stained with hematoxylin and eosin. Nonatretic growing follicles were counted in every fifth section. The number of small preantral (20-170 µm), large preantral (171-220 µm), small antral (221-310 µm), and large antral (>311 µm) was combined to yield the total number of nonatretic growing follicles.

Hormone Measurements

Estradiol was measured by immunoassay. After ethyl ether extraction, serum mouse 17β-estradiol (E2) was measured by enzyme-linked immunosorbent assay (ELISA) kit in duplicate according to the manufacturer recommendations (Cat# SE 120084, RRID:AB_2827635, Sigma-Aldrich, Saint-Quentin Fallavier, France). The standard range was as follows: 0, 3, 10, 30, 100, and 300 pg/mL. The antibody is a polyclonal anti-estradiol antibody, coated on microwells (25). Anti-E2 antibody coated wells were incubated with E2 standards, controls, samples, and E2 enzyme conjugate. During the incubation, a fixed amount of HRP-labeled E2 competes with the endogenous E2 in the standards, samples, or control sera for a fixed number of binding sites of the specific E2 antibody. E2 Peroxidase Conjugate immunologically bound to the well progressively decreases as the concentration of E2 in the specimen increases. Then unbound E2 Peroxidase Conjugate was removed and the wells were washed. After a second incubation with a solution of TMB, the color development was stopped and the absorbance was measured spectrophotometrically at 450 nm. Quality control samples were provided by Probioqual (Lyon, France) and as "blank" control we used serum from prepubertal mice. Accuracy did not differ from 100%. The detection limit was 1 pg/mL. Intra- and inter-assay precision were, respectively, 15% and 20% at the concentration of 1 pg/mL, 8% and 10% at 4 pg/mL, and 5% and 8% at 7 pg/mL.

Other steroid hormones were characterized using liquid chromatography-tandem mass spectrometry (LC-MS/MS) as described previously (26). One hundred µL of serum (sample or quality control) were vortex-mixed with 20 µL of the internal standard solution (a mix of testosterone-1a,2a-D2 and progesterone-1a,2a-D2) and 1.5 mL ethyl ether for 3 minutes. The solutions were then allowed to stand for 20 minutes, when the supernatants were separated and evaporated to dryness at room temperature under a stream of nitrogen. The dried extracts were reconstituted in 100 µL MeOH/water (55/45; V/V). The samples were injected into an Acquity UPLC system (Waters, Manchester, UK), equipped with an Acquity UHPLC HSST3 column (Waters, Guyancourt, France). The mobile phase consisted of a mixture of water and MeOH. It was operated with a flow rate of 0.5 mL/min in gradient mode, at a temperature of 40 °C. Mass spectra were recorded using a Quattro Premier triple quadrupole mass spectrometer (Waters, Manchester, UK). Measurements were performed using positive electrospray ionization (ESI) in Multiple Reaction Monitoring (MRM) data-acquisition mode. The parameters of the electrospray interface were optimized as follows: capillary voltage 4 kV, source temperature 120 °C, desolvation temperature 350 °C, desolvation gas 900 L/hour.

Steroid identification was based on an identical retention time and 2 identical mass transitions with authentic reference compounds (testosterone from Sigma-Aldrich, and progesterone from Vetranal). Quantification was performed relative to a calibration series (0, 0.1 to 100 ng/mL of each steroid) with an appropriate internal standard steroid. All measurements were performed in duplicate. Data processing was ensured using MassLynx software (V 4.1, SCN 805, Waters, Manchester, UK). A QuantLynx (V 4.1, SCN 803, Waters) was used to detect and integrate the peaks. Accuracy checked in our unit did not differ from 100%. Detection limits were 0.06 nmol/L for testosterone and 0.1 nmol/L for progesterone. Intra-assay coefficients of variation for these steroids were < 10% at detection level, and < 8% throughout the range of observed values. Inter-assay coefficients of variation were < 12% throughout the range of observed values.

Serum levels of inhibin A and B were measured using the multi-species Ansh Lab's ELISAs (Ansh Labs Cat# AL-161, RRID:AB_2783699; Ansh Labs Cat# AL-163, RRID: AB_2783700).

Micro Computed Tomography Analysis

Femurs were scanned at a resolution of 9 µm, using a SkyScan 1076 system (Bruker, Kontich, Belgium) in a blinded fashion. According to the published guidelines (27), the following settings were used: x-ray power and tube current were 40 kV and 250 µA, respectively. Beam hardening was reduced using a 1-mm aluminum filter, exposure time was 2.3 seconds, and an average of 3 pictures was taken at each angle with steps of 0.8° to generate final images. Segmentation of the reconstructed images was done on basis of global thresholding. Using software packages from Bruker (NRecon, CtAn, and Dataviewer), bone microarchitecture parameters were assessed in trabecular and cortical bones of all mice (n = 8-12 mice per genotype and sex). The trabecular bone parameters trabecular bone volume fraction (BV/TV), trabecular thickness (Tb.Th), trabecular number (Tb.N), trabecular separation (Tb.Sp), trabecular patterning factor (Tb.Pf) and structure model index (SMI; 0 = plate-like, 3 = rod-like) were determined in the distal metaphysis of the femur (region of interest [ROI] of 0.9 mm from distal growth plate toward diaphysis). For 16-month-old femurs, the trabecular compartment was manually selected due to the porous nature of the bones. In the mid-diaphysis (ROI of 0.45 mm), tissue area (Tt.Ar), cortical area (Ct.Ar), marrow area (Ma.Ar), cortical thickness (Ct.Th), periosteal perimeter (Ps.Pm) and moment of inertia (MOI) were analyzed. All ROIs were corrected for length of the femurs.

Histomorphometry of Femurs

Femurs of 10-month-old female mice (n = 4-7 mice per genotype) were routinely embedded in methylmetacrylate as described before (28). Sections of 6 µm were deacrylated, hydrated, and subjected to Goldner's Masson Trichrome staining. Briefly, sections were subsequently stained in hematoxylin/ferric chloride, ponceau de xylidine/acid fuchsin, orange G, and Light green solutions as described previously in detail (29). The sections were dehydrated and embedded in Entellan (Electron Microscopy Sciences, Hatfield, PA, USA). Images were taken using a NanoZoomer system and analyzed using NDP viewer (Nanozoomer 2.0 HT, Hamamatsu). Categorized bone marrow adiposity measurements based on the amount of bone marrow fat cells were performed in a blinded fashion. The following score system was used: 0 = near or complete absence of bone marrow fat cells; 1 = presence of bone marrow fat cells occupying less than half of the bone marrow cavity; 2 = presence of bone marrow fat cells occupying more than half of the bone marrow cavity; and 3 = presence of bone marrow fat cells filling nearly the entire bone marrow cavity.

Statistical Analysis

Steroid hormone levels during the estrous cycle were analyzed by two-way analysis of variance (ANOVA) followed by Bonferroni post hoc analysis. All other parameters were analyzed by one-way ANOVA followed by Tukey HSD post hoc test. To determine an effect of aging linear regression analysis was performed. Analyses were performed using GraphPad Prism 9 (GraphPad Software, Inc.). A P value <0.05 was considered significant. Data are expressed as mean ± SEM.

Results

General Characteristics of Mice

At 2 months of age, female AMHKO mice were slightly, but significantly, heavier than WT mice ($P < 0.05$). However, at subsequent ages, the analyzed body weight of female AMHKO and MRKI mice did not differ from WT mice (Fig. 1A). In agreement with our previous studies (23, 24), female AMHKO mice had an increased number of growing follicles at 2 and 4 months of age ($P < 0.001$ and $P < 0.01$, respectively) and a reduced number or no growing follicles at 10 and 16 months of age compared with WT mice ($P < 0.001$ and $P < 0.01$, respectively) (Fig. 1A). Ovaries of female MRKI mice showed a similar pattern as AMHKO mice, with increased follicle numbers at 2 and 4 months ($P < 0.05$) and severely reduced numbers at the older ages ($P < 0.001$ and $P < 0.05$ at 10 and 16 months, respectively) (Fig. 1A). In line with this, the ovarian weight of AMHKO and MRKI mice was significantly increased at 2 and 4 months of age and significantly reduced at 10 and 16 months of age compared with WT mice (Fig. 1A). Given the increased follicle number in AMHKO and MRKI mice at the reproductive ages, we also determined estradiol and progesterone levels throughout the estrous cycle at 4 months of age. Both estradiol and progesterone levels showed the expected estrous variation but did not differ between genotypes. Also, testosterone levels did not significantly differ between the genotypes during the estrous cycle (Fig. 1B). In agreement, and confirming previous results in AMHKO mice (23), no difference in length or regularity of the cycle was observed between the genotypes.

For male mice, body weight of AMHKO and MRKI mice did not differ from WT mice (Fig. 1C). Testes of AMHKO and MRKI mice were significantly heavier compared with WT mice at all ages analyzed. Gross morphological analysis confirmed the previously reported presence of all stages of spermatogenesis and the appearance of empty seminiferous tubules with increasing age due to focal atrophy of the germinal epithelium (20)(results not shown). However, testosterone levels did not significantly differ between genotypes, although large variation in levels was observed within the groups (Fig. 1D).

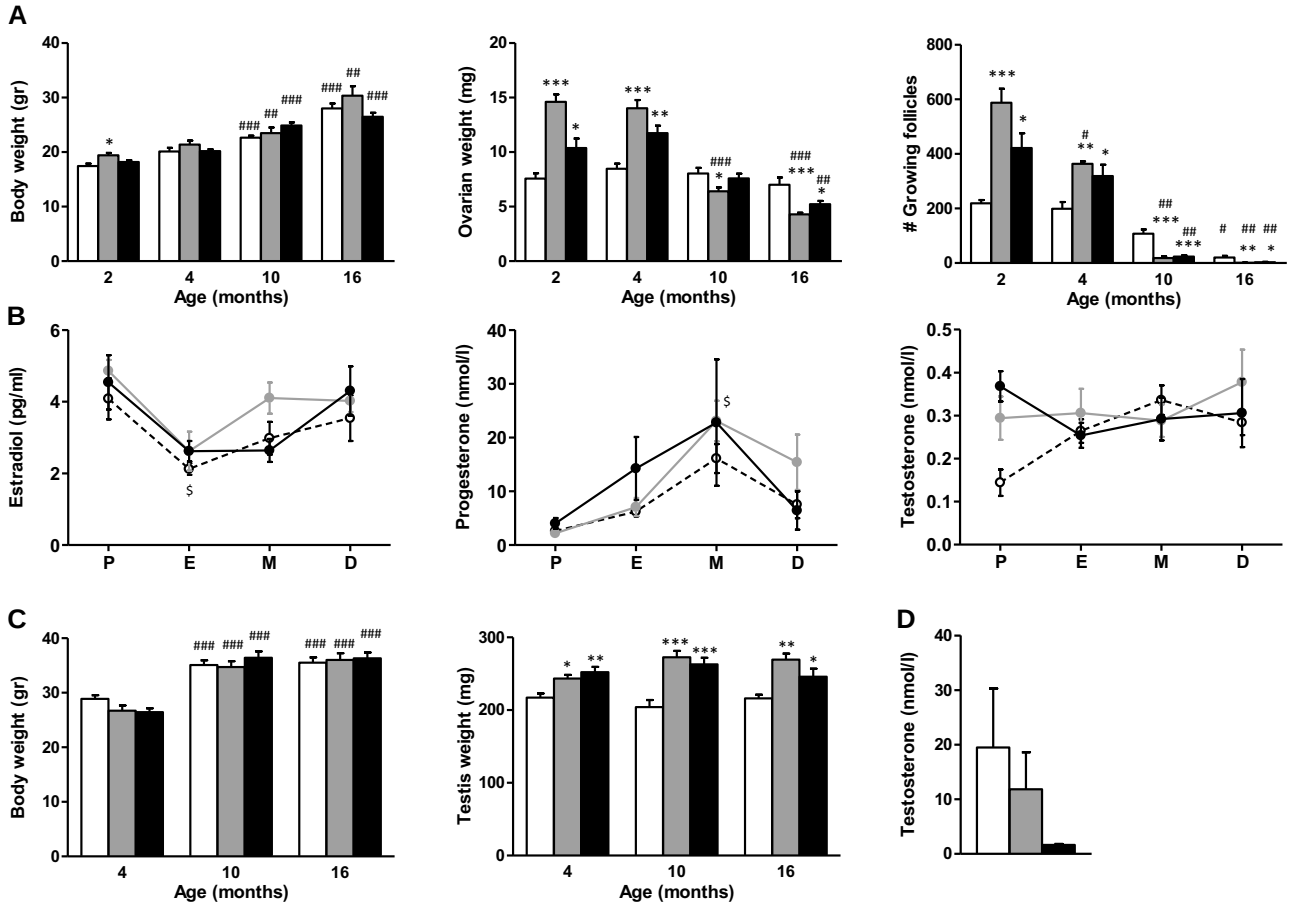

Figure 1. General characteristics and sex steroid hormone levels in WT and AMH signaling deficient mice. (A) Body weight, ovarian weight, and number of growing follicles in 2-, 4-, 10-, and 16-month-old female WT (white bars), AMHKO (gray bars), and MRKI (black bars) mice (n = 8-10). (B) Estradiol, progesterone, and testosterone levels during the estrous cycle in 4-month-old WT (dotted black line), AMHKO (solid gray line), and MRKI (solid black line) mice (n = 5 per cycle day). Abbreviations: P, pro-estrus; E, estrus; M, metestrus; D, di-estrus. $^{\$}P < 0.05$, vs pro-estrus of same genotype. (C) Body weight and testis weight in 4-, 10-, and 16-month-old male mice (n = 8-10). (D) Testosterone levels in 4-month-old male WT (white bars), AMHKO (gray bars), and MRKI (black bars) mice (n = 6-7). Data are presented as mean ± SEM, $^{*}P < 0.05$, $^{**}P < 0.01$, $^{***}P < 0.001$ vs WT mice of the same age. $^{\#}P < 0.05$, $^{\#\#}P < 0.01$, $^{\#\#\#}P < 0.001$ vs 2-month-old mice of the same genotype.

Micro Computed Tomography Analysis

Aging effects were examined, and WT mice showed the expected age-dependent changes in bone parameters. Both female and male WT mice showed an age-dependent decline in BV/TV (linear trend: $P < 0.001$). Further, in both female and male knockout models, trabecular bone was lost with increasing age (linear trend: both $P < 0.001$ [females: Supplementary Fig. 2A and males: Supplementary Fig. S1] (30)). However, female MRKI mice had a higher BV/TV compared with WT mice at the age of 2 months ($P < 0.001$). This increased value could be explained by a significant increase in both trabecular thickness and number (both $P < 0.001$) (Fig. 2B and 2C). The higher BV/TV in MRKI mice compared with WT mice persisted at the age of 4 and 10 months. At the age of 10 months, this increase was explained by a significant higher trabecular thickness in both knockout models ($P < 0.05$ and $P < 0.001$ in AMHKO and MRKI mice, respectively) (Fig. 2B). At 16 months of age, BV/TV in female AMHKO and MRKI mice was similar to that of WT mice due to a greater decrease in trabecular bone between 10 and 16 months of age in both AMHKO and MRKI mice compared with WT mice (Fig. 2A). The decrease in trabecular bone was more pronounced in AMHKO mice, leading to a significantly different BV/TV between AMHKO and MRKI mice ($P < 0.05$). This difference between genotypes was best explained by a significantly lower trabecular thickness in AMHKO mice compared with both WT and MRKI mice at 16 months of age ($P < 0.05$ and $P < 0.01$, respectively) (Fig. 2B).

Concerning cortical bone, we observed an age-dependent increase in marrow area in both female and male WT mice (linear trend: both $P < 0.001$). A gradual increase of the periosteal perimeter was observed in female WT mice between 2 and 16 months of age (linear trend: $P < 0.001$) and also in male WT mice between 4 and 16 months of age (linear trend: $P < 0.001$). Both knockout models showed a similar pattern of aging as the WT mice (female: Fig. 3 and male: Supplementary Fig. S2 (30)). However, differences between female WT and knockout mice were observed at 10 months of age. At this age, female MRKI mice had a significantly higher cortical area and marrow area compared with WT mice (both $P < 0.01$). As a result, the periosteal perimeter and moment of inertia of MRKI mice was also higher (both $P < 0.001$) (Fig. 3 and Table 1).

The bone phenotype of both male knockout models resembled that of WT mice at all ages studied. There were no significant differences between the genotypes for any of the trabecular bone parameters (Supplementary Fig. S1 and

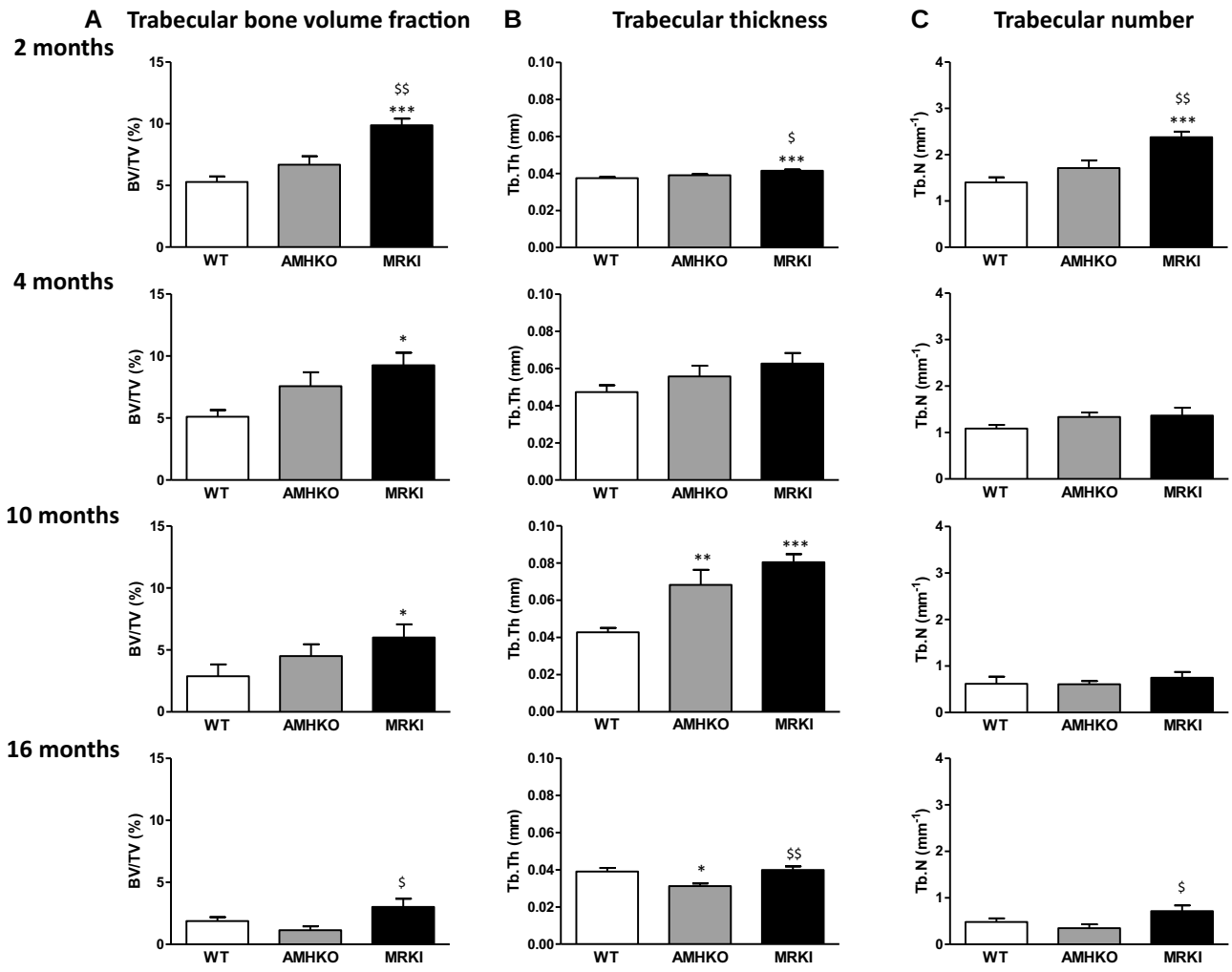

Figure 2. Trabecular bone parameters in WT and AMH signaling deficient female mice. Trabecular bone microarchitecture in 2-, 4-, 10- and 16-month-old female WT (white bars), AMHKO (gray bars) and MRKI (black bars) mice analyzed using microCT (n = 8-10). (A) Trabecular bone volume fraction, (B) Trabecular thickness, (C) Trabecular number. Data are presented as mean ± SEM, $^{*}P < 0.05$, $^{***}P < 0.001$ vs WT mice of the same age, $^{\$}P < 0.05$ vs AMHKO mice, $^{\$\$}P < 0.01$ vs AMHKO mice.

Supplementary Table S1 (30)). Regarding cortical bone parameters, we only observed a significantly smaller cortical area in AMHKO mice at the age of 10 months compared with WT mice ($P < 0.05$) (Supplementary Fig. S2 and Supplementary Table S1 (30)).

Inhibin A and B Levels in Female AMH Signaling Deficient Mice

The increased trabecular bone at reproductive age combined with enhanced loss of trabecular bone at older ages in AMHKO and MRKI mice correlates with the change in growing follicle number at these ages. Therefore, we measured serum levels of inhibin A and B, since these gonadal growth factors have been shown to have regenerative effects on bone.

Throughout the estrous cycle at 4 months of age, inhibin A levels showed the expected estrous variation but did not differ between genotypes (Fig. 4A). At 2 and 10 months of age in samples randomly collected throughout the cycle, inhibin A levels were similar between genotypes, although large variation within genotypes may have masked potential differences. However, at 16 months of age, inhibin A levels were significantly lower in AMHKO and MRKI mice compared with WT mice ($P < 0.05$). Furthermore, in AMHKO mice, inhibin A levels in the aged mice were significantly lower compared to young mice ($P < 0.001$) (Fig. 4B).

For inhibin B levels, we observed that at 4 months of age, levels were increased at estrus in AMHKO and MRKI ($P < 0.001$ and $P < 0.05$ respectively), while no differences were observed at the other days of the estrous cycle (Fig. 4C). In samples collected randomly throughout the cycle, inhibin B levels did not differ between genotypes at 2 months of age. However, at 10 and 16 months of age, inhibin B levels were significantly lower in AMHKO and MRKI mice compared with WT mice ($P < 0.001$). In all 3 genotypes, inhibin B levels declined with increasing age. However, in AMHKO and MRKI mice significantly lower levels were already observed at 10 months of age ($P < 0.05$ and $P < 0.001$, respectively), while in WT mice a significant difference was only observed at 16 months of age ($P < 0.01$) when compared with 2-month-old mice of the same genotype (Fig. 4D).

Histomorphometry of Femurs

Goldner's staining of femurs from 10-month-old female mice confirmed the observed differences in trabecular bone volume

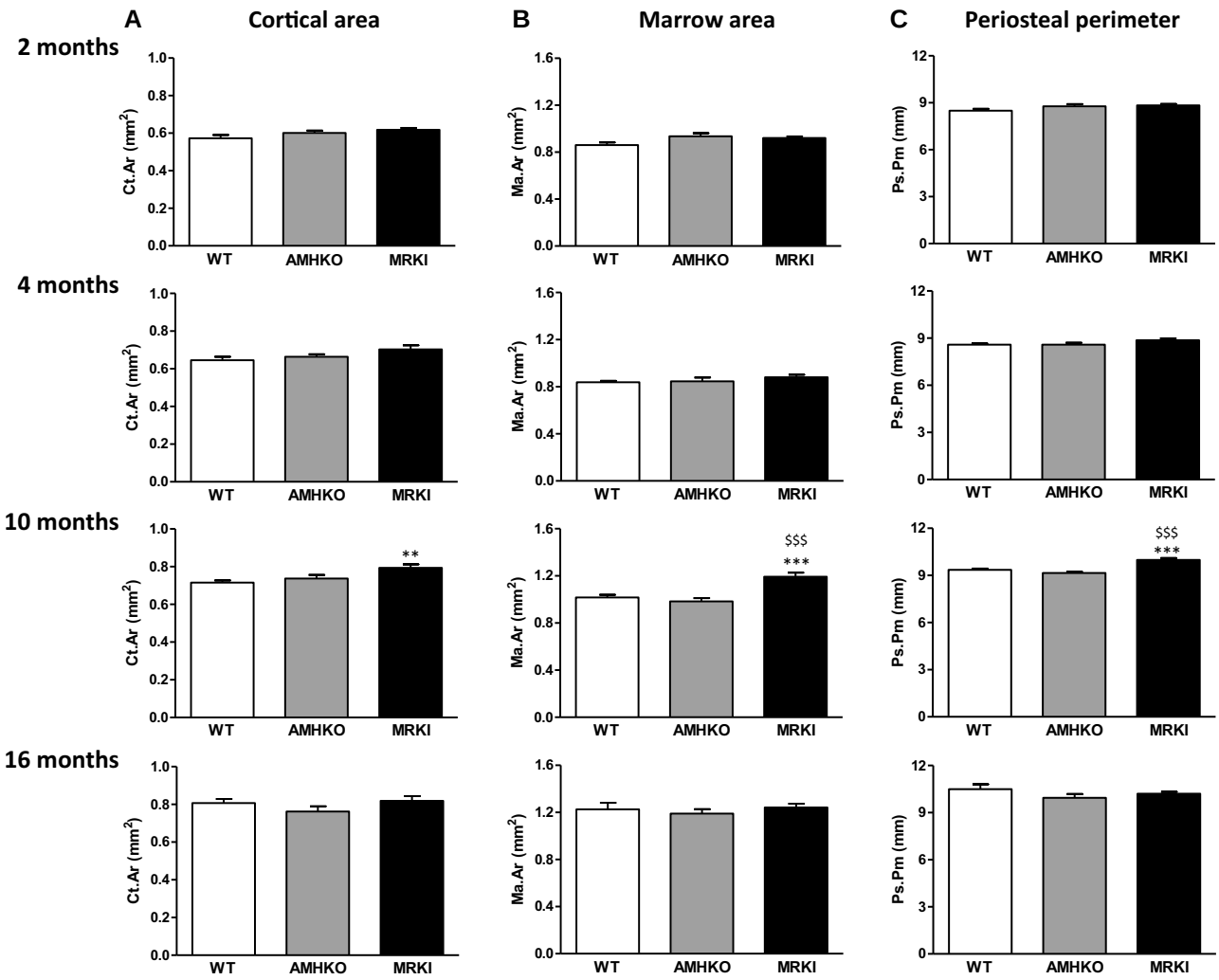

Figure 3. Cortical bone parameters in WT and AMH signaling deficient female mice. Cortical bone microarchitecture in 2-, 4-, 10-, and 16-month-old female WT (white bars), AMHKO (gray bars), and MRKI (black bars) mice analyzed using microCT (n = 8-10). (A) Cortical area, (B) Marrow area, (C) Periosteal perimeter. Data are presented as mean ± SEM, $^{*}P < 0.05$, $^{**}P < 0.01$, $^{***}P < 0.001$ vs WT mice of the same age, $^{\$\$\$}P < 0.001$ vs AMHKO mice.

between the genotypes (Fig. 5A). Interestingly, clear differences were observed in bone marrow adiposity between genotypes: 4 out of 7 femurs of female AMHKO mice contained very few bone marrow adipocytes in the bone marrow cavity, while none of the WT or MRKI mice displayed this phenotype (Fig. 5B).

Discussion

In this study, we investigated the effect of AMH signaling deficiency on bone. Female AMHKO and MRKI mice had increased trabecular bone compared with WT mice up to the age of 10 months, but this difference disappeared at 16 months of age. As shown by an increased marrow area and periosteal perimeter, MRKI mice displayed advanced cortical aging at 10 months of age compared with WT mice. Furthermore, we observed that female AMHKO mice of 10 months of age had remarkably few bone marrow adipocytes in their bone marrow cavity compared with the other genotypes.

Previously, we demonstrated that AMH deficiency results in a gradual but accelerated ovarian aging (23). In this study, we observed that MRKI mice, an AMHR2 deficient model, display a similar ovarian aging phenotype. Therefore, we hypothesized that mice lacking AMH signaling could serve as a model for osteoporosis following natural menopause. Postmenopausal osteoporosis is characterized by a reduced trabecular bone mass and cortical thinning (8, 11). Despite advanced depletion of the ovarian follicle pool compared to WT mice, at 16 months of age, bone parameters of female AMHKO and MRKI mice did not largely differ from female WT mice. In contrast, young female AMHKO and MRKI mice had more trabecular bone than WT mice. Combined with the relatively normal bone parameters at advanced age, this suggests that deficiency in AMH signaling causes accelerated bone loss after a critical age. Indeed, both female knockout models displayed a greater decrease in trabecular bone between 10 and 16 months of age compared with WT mice.

In OVX mice, which constitute the most commonly used model for postmenopausal bone loss, trabecular bone architecture and cortical bone area decline soon after ovariectomy (12). Chemically induced menopause by 4-vinylcyclohexene diepoxide (VCD) in mice also resulted in a decrease in trabecular bone parameters. However, in contrast to OVX mice,

Table 1. Trabecular and cortical bone parameters in WT and AMH signaling deficient female mice

	2 months			4 months			10 months			16 months		
	WT	AMHKO	MRKI	WT	AMHKO	MRKI	WT	AMHKO	MRKI	WT	AMHKO	MRKI
Tb.Sp (mm)	0.28 ± 0.02	0.24 ± 0.03	0.17 ± 0.01**	0.34 ± 0.02	0.26 ± 0.02	0.27 ± 0.04	0.81 ± 0.13	0.63 ± 0.08	0.50 ± 0.04	0.94 ± 0.02	1.48 ± 0.03	0.72 ± 0.01$^{\$}$
Tb.Pf (mm^{-1})	45.6 ± 1.2	42.0 ± 1.7	33.9 ± 0.9***,$$$	37.4 ± 1.5	30.5 ± 2.7	29.0 ± 2.5*	39.7 ± 3.0	32.9 ± 2.6	25.4 ± 2.5**	48.2 ± 2.4	61.9 ± 3.5**	45.2 ± 3.0$^{\$\$}$
SMI	2.5 ± 0.0	2.4 ± 0.1	2.1 ± 0.0***,$$	2.6 ± 0.1	2.4 ± 0.1	2.5 ± 0.1	2.5 ± 0.1	2.8 ± 0.1	2.6 ± 0.2	2.7 ± 0.1	2.8 ± 0.0	2.6 ± 0.1
Ct.Th (mm)	0.14 ± 0.00	0.14 ± 0.00	0.14 ± 0.00	0.15 ± 0.00	0.16 ± 0.00	0.16 ± 0.00	0.15 ± 0.00	0.16 ± 0.00	0.16 ± 0.00	0.15 ± 0.00	0.14 ± 0.01	0.16 ± 0.01
MOI (mm^4)	0.22 ± 0.01	0.25 ± 0.01	0.25 ± 0.01	0.25 ± 0.01	0.26 ± 0.01	0.29 ± 0.02	0.32 ± 0.01	0.32 ± 0.01	0.41 ± 0.02***,$$$	0.43 ± 0.03	0.38 ± 0.02	0.43 ± 0.02
Tt.Ar (mm^2)	1.43 ± 0.04	1.54 ± 0.04	1.54 ± 0.02	1.48 ± 0.03	1.51 ± 0.03	1.58 ± 0.4	1.73 ± 0.03	1.72 ± 0.03	1.99 ± 0.05***,$$$	2.03 ± 0.07	1.95 ± 0.04	2.06 ± 0.05

Trabecular and cortical bone microarchitecture in 2-, 4-, 10-, and 16-month-old female WT, AMHKO and MRKI mice analyzed using micro computed tomography (microCT) (n = 8-10); data are presented as mean ± SEM.
Abbreviations: Ct.Th, cortical thickness; MOI, moment of inertia; SMI, structure model index; Tb.Pf, trabecular patterning factor; Tb.Sp, trabecular separation; Tt.Ar, tissue area.
*$P < 0.05$ vs WT mice, **$P < 0.01$ vs WT mice, ***$P < 0.001$ vs WT mice, $^{\$}P < 0.05$ vs AMHKO mice, $^{\$\$}P < 0.01$ vs AMHKO mice, $^{\$\$\$}P < 0.001$ vs AMHKO mice.

cortical bone parameters were not affected (31). This is in agreement with our results, in which we only observed effects on trabecular bone but not cortical bone upon AMH signaling deficiency. In their study, Wright et al (31) suggested that, although both OVX and chemically induced menopause ablate estrogen production, the presence of residual ovarian tissue in the VCD-treated mice attenuates bone loss. Also, in both AMH signaling deficient models ovaries remain present. However, there are also important differences between our mouse models and the chemically induced mouse model of ovarian failure. In female AMHKO and MRKI mice, the increased loss of trabecular bone was only observed after 10 months of age, which correlated with the significant reduced number of follicles at this age. In the study of Wright et al (31), ovarian failure was induced at 1 month of age, and bone architecture was affected 3 months thereafter. Importantly, VCD treatment causes a rapid depletion of primordial and primary follicles, subsequently resulting in a decline in preantral and small antral follicles (32). Thus, there is a clear difference in the timing of bone loss. Another important difference is the dynamic of follicle loss. Although AMH signaling deficient mice also have an accelerated depletion of primordial follicles, this process is gradual and furthermore is paralleled with an increase in the number of preantral follicles in mice of 2- to 4-months of age. This increase in number of growing follicles, and thereby altered levels of gonadal growth factors, may likely explain the increase in trabecular bone observed during the early reproductive period of our mice.

We previously showed that the increased number of growing follicles does not affect ovulation rate (24). In agreement, we now show that in AMHKO and MRKI mice estrogen and progesterone levels during the estrous cycle are not affected. Likewise, testosterone levels did not differ between genotypes during the estrous cycle, although levels appeared elevated at pro-estrus in the AMH signaling deficient mice. Although sex steroids are important hormones in bone homeostasis, the ovary also produces other ovarian factors, which potentially may affect bone metabolism. For instance, the gonadal growth factors inhibin and activin have been shown to have direct effects on both osteoblasts and osteoclasts in primary murine bone marrow cultures (33). Overexpression of inhibin A in mice resulted in an increased bone mineral density and bone volume (34). In our study, inhibin A levels of mice of reproductive age did not differ between genotypes. Given that inhibin A is mainly produced by pre-ovulatory follicles (35), this is in line with the normal number of pre-ovulatory follicles in AMHKO and MRKI mice. However, inhibin B levels were increased at estrus in AMHKO and MRKI mice, confirming our previous study in which a 2-fold increase in inhibin levels was observed in 4-month-old AMHKO mice at estrus (23). Since inhibin B is mainly produced by the earlier stages of follicular growth (35), this increase at estrus likely reflects the increased and earlier cyclic recruitment of growing follicles, previously described for AMHKO mice (24). Interestingly, the age-dependent decline in inhibin B levels was accelerated in AMHKO and MRKI mice, correlating with the earlier decline in number of growing follicles. We also noted that inhibin A levels were decreased in aged AMHKO and MRKI mice, suggesting cessation of ovulations at an earlier age. These findings show that changes in follicle dynamics in these mice result in concomitant changes in circulating ovarian growth factors. Whether inhibins account for the increased

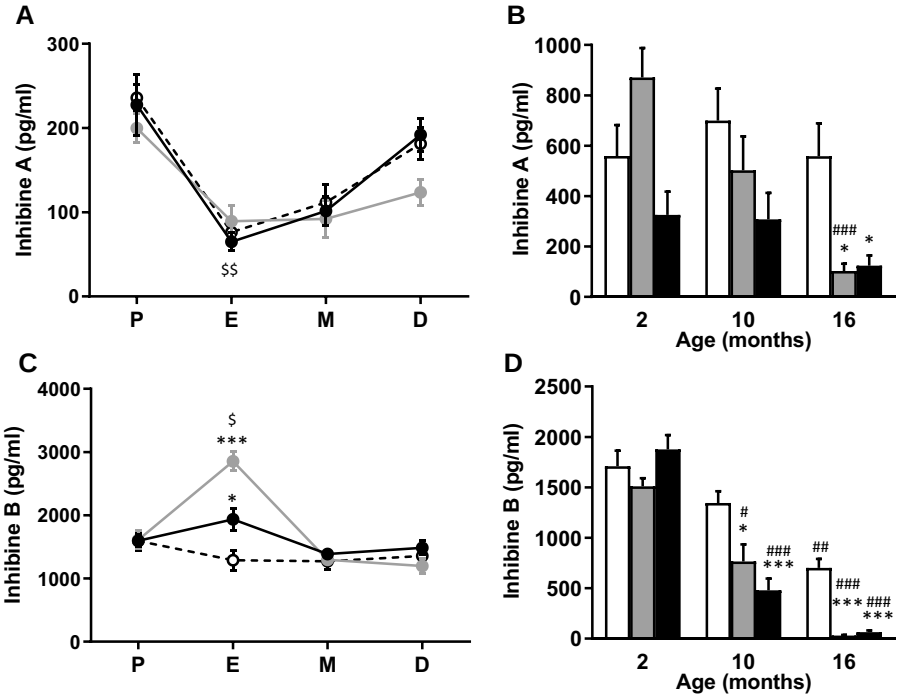

Figure 4. Inhibin A and B levels in WT and AMH signaling deficient mice. (A) Inhibin A and (C) Inhibin B levels during the estrous cycle in 4-month-old WT (dotted black line), AMHKO (solid gray line), and MRKI (solid black line) mice (n = 5 per cycle day). Abbreviations: P, pro-estrus; E, estrus; M, metestrus; D, di-estrus. Data are presented as mean ± SEM. $^{*}P < 0.05$, $^{***}P < 0.001$ vs WT mice of same cycle day; $^{\$}P < 0.05$, $^{\$\$}P < 0.01$ vs pro-estrus day of the same genotype. (B) Inhibin A and (D) inhibin B levels in 2-, 10-, and 16-month-old female WT (white bars), AMHKO (gray bars), and MRKI (black bars) mice (n = 8-10). Data are presented as mean ± SEM. $^{*}P < 0.05$, $^{***}P < 0.001$ vs WT mice of same age. $^{\#}P < 0.05$, $^{\#\#}P < 0.01$, $^{\#\#\#}P < 0.001$ vs 2-month-old mice of same genotype.

trabecular bone at reproductive age and accelerated bone loss with increasing age in AMHKO and MRKI mice remains to be determined. However, our results support findings of a cross-sectional age-stratified study of pre- and postmenopausal women, in which it was shown that serum inhibin A and inhibin B levels inversely correlated with bone turnover markers and had better predictive value than follicle-stimulating hormone (FSH) and E2, particularly in pre- and perimenopausal women (36). Other reproductive hormones may also contribute to the regulation of bone metabolism. As reviewed by Mills et al (37), hypothalamic and pituitary hormones, such as kisspeptin, gonadotropin-releasing hormone, and FSH, have been implicated. The recent discovery that AMH may regulate GnRH pulsatility (38) suggests that the effect of AMH signaling deficiency on bone could potentially also be mediated via regulation of the hypothalamic-pituitary-gonadal axis. Unfortunately, we were unable to measure FSH and estradiol levels in the aged mice due to insufficient serum volume. However, changes in FSH and estradiol occur relatively late during reproductive aging (39), suggesting that changes in circulating levels of gonadal growth factors may contribute to altered bone turnover during the early phase of reproductive aging.

The observed effect of AMH signaling deficiency on bone appeared to be sex-dependent, since in male AMHKO and MRKI mice the trabecular and cortical bone parameters were comparable to WT mice. This sex-specific effect supports an indirect effect of AMH on bone homeostasis through other ovarian growth factors or hypothalamic/pituitary hormones. However, in a recent study, AMH was shown to inhibit

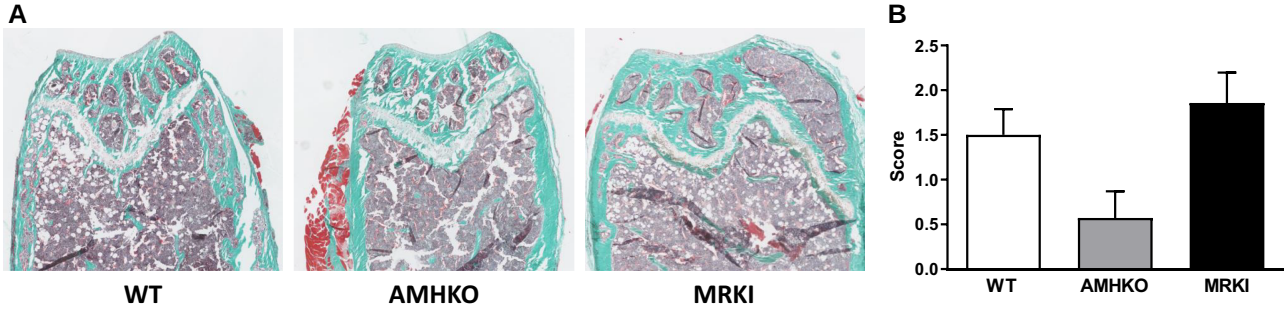

Figure 5. Histomorphometry in WT and AMH signaling deficient female mice. (A) Histomorphometry in 10-month-old female WT and AMH signaling deficient mice performed using Goldner's staining. (B) Categorized bone marrow adiposity measurements. WT (white bars), AMHKO (gray bars), and MRKI (black bars) (n = 4-7). Data are presented as mean ± SEM.

TRAP-positive multinuclear osteoclast differentiation in osteoclast precursor cells, derived from mouse bone marrow cells (40). Thus, further research is required to elucidate these differences between in vivo and in vitro effects of AMH on bone cells.

Histomorphometric analysis revealed differences in bone marrow adiposity between the genotypes. At 10 months of age, in more than 50% of the female AMHKO mice analyzed, very few bone marrow adipocytes were present in the bone marrow cavity of their femurs. Thus, female AMHKO mice seem to have increased osteogenesis and decreased adipogenesis. This phenotype was only observed in AMHKO mice and not in the MRKI mice. This phenotype is also remarkable, since during and after menopause normally a transition from osteogenesis to adipogenesis occurs (41-43), and thus further studies are required. The finding that AMH and AMHR2 deficiency differentially affect mesenchymal stem cell differentiation may imply that AMHR2 can signal independent from AMH. However, this is highly speculative as AMHKO and MRKI mice are phenocopies concerning Müllerian duct regression and ovarian phenotype.

In conclusion, loss of AMH signaling resulted in an advanced loss of trabecular bone. However, due to an increased bone mass at early reproductive life, which coincided with an increased number of growing follicles, bone parameters of aged female AMHKO and MRKI mice did not largely differ from aged WT mice despite advanced ovarian aging. Although the bone phenotype in mice lacking AMH signaling does not directly resemble menopause-related osteoporosis in humans, our results suggest that mice deficient in AMH signaling may be an interesting model to identify reproductive hormones and their mode of action beyond estrogen that contribute to bone homeostasis.

Acknowledgments

We thank Romy Trouerbach for technical assistance.

Funding

Departmental funding.

Data Availability

Some or all datasets generated during and/or analyzed during the current study are not publicly available but are available from the corresponding author on reasonable request.

Disclosures

C.v.A., M.K., A.McL., P.K., N.L., and B.C.J.v.d.E. have nothing to declare. J.A.V. has received royalties from AMH assays, paid to the institute/lab with no personal financial gain.

References

1. Compston JE, McClung MR, Leslie WD. Osteoporosis. *Lancet*. 2019;393(10169):364-376.
2. NIH Consensus Development Panel on Osteoporosis Prevention, Diagnosis, and Therapy. Osteoporosis prevention, diagnosis, and therapy. *JAMA*. 2001;285(6):785-795.
3. Hernlund E, Svedbom A, Ivergård M, *et al*. Osteoporosis in the European Union: medical management, epidemiology and economic burden. A report prepared in collaboration with the International Osteoporosis Foundation (IOF) and the European Federation of Pharmaceutical Industry Associations (EFPIA). *Arch Osteoporos*. 2013;8(1-2):136.
4. Melton LJ III, Chrischilles EA, Cooper C, Lane AW, Riggs BL. How many women have osteoporosis? JBMR Anniversary Classic. JBMR, Volume 7, Number 9, 1992. *J Bone Miner Res*. 2005;20(5):886-892.
5. Riggs BL, Melton LJ III, Robb RA, *et al*. Population-based study of age and sex differences in bone volumetric density, size, geometry, and structure at different skeletal sites. *J Bone Miner Res*. 2004;19-(12):1945-1954.
6. Riggs BL, Melton LJ, Robb RA, *et al*. A population-based assessment of rates of bone loss at multiple skeletal sites: evidence for substantial trabecular bone loss in young adult women and men. *J Bone Miner Res*. 2008;23(2):205-214.
7. Weitzmann MN, Pacifici R. Estrogen deficiency and bone loss: an inflammatory tale. *J Clin Invest*. 2006;116(5):1186-1194.
8. Eastell R, O'Neill TW, Hofbauer LC, *et al*. Postmenopausal osteoporosis. *Nat Rev Dis Primers*. 2016;2(1):16069.
9. Garnero P, Sornay-Rendu E, Chapuy M-C, Delmas PD. Increased bone turnover in late postmenopausal women is a major determinant of osteoporosis. *J Bone Miner Res*. 1996;11(3):337-349.
10. Manolagas SC, O'Brien CA, Almeida M. The role of estrogen and androgen receptors in bone health and disease. *Nat Rev Endocrinol*. 2013;9(12):699-712.
11. Szulc P, Seeman E, Duboeuf F, Sornay-Rendu E, Delmas PD. Bone fragility: failure of periosteal apposition to compensate for increased endocortical resorption in postmenopausal women. *J Bone Miner Res*. 2006;21(12):1856-1863.
12. Komori T. Animal models for osteoporosis. *Eur J Pharmacol*. 2015;759:287-294.
13. Roberts BC, Giorgi M, Oliviero S, Wang N, Boudiffa M, Dall'Ara E. The longitudinal effects of ovariectomy on the morphometric, densitometric and mechanical properties in the murine tibia: a comparison between two mouse strains. *Bone*. 2019;127:260-270.
14. Wang H, Zhou K, Xiao F, *et al*. Identification of circRNA-associated ceRNA network in BMSCs of OVX models for postmenopausal osteoporosis. *Sci Rep*. 2020;10(1):10896.
15. te Velde ER, Scheffer GJ, Dorland M, Broekmans FJ, Fauser BC. Developmental and endocrine aspects of normal ovarian aging. *Mol Cell Endocrinol*. 1998;145(1-2):67-73.
16. Mayer LP, Devine PJ, Dyer CA, Hoyer PB. The follicle-deplete mouse ovary produces androgen. *Biol Reprod*. 2004;71(1): 130-138.
17. Fogle RH, Stanczyk FZ, Zhang X, Paulson RJ. Ovarian androgen production in postmenopausal women. *J Clin Endocrinol Metab*. 2007;92(8):3040-3043.
18. Hall JE. Endocrinology of the menopause. *Endocrinol Metab Clin North Am*. 2015;44(3):485-496.
19. Finch CE. The menopause and aging, a comparative perspective. *J Steroid Biochem Mol Biol*. 2014;142:132-141.
20. Mishina Y, Rey R, Finegold MJ, *et al*. Genetic analysis of the Mullerian-inhibiting substance signal transduction pathway in mammalian sexual differentiation. *Genes Dev*. 1996;10(20): 2577-2587.
21. Arango NA, Lovell-Badge R, Behringer RR. Targeted mutagenesis of the endogenous mouse Mis gene promoter: in vivo definition of genetic pathways of vertebrate sexual development. *Cell*. 1999;99(4):409-419.
22. Visser JA, de Jong FH, Laven JS, Themmen AP. Anti-Mullerian hormone: a new marker for ovarian function. *Reproduction*. 2006;131(1):1-9.
23. Durlinger AL, Kramer P, Karels B, *et al*. Control of primordial follicle recruitment by anti-mullerian hormone in the mouse ovary. *Endocrinology*. 1999;140(12):5789-5796.
24. Visser JA, Durlinger AL, Peters IJ, *et al*. Increased oocyte degeneration and follicular atresia during the estrous cycle in anti-Mullerian hormone null mice. *Endocrinology*. 2007;148(5): 2301-2308.

25. Chakravarthi VP, Ghosh S, Roby KF, Wolfe MW, Rumi MAK. A gatekeeping role of ESR2 to maintain the primordial follicle reserve. *Endocrinology*. 2020;161(4):bqaa037.
26. Menet MC, Hebert-Schuster ML, Lahlou N, *et al*. rFSH in medically assisted procreation: evidence for ovarian follicular hyperplasia and interest of mass spectrometry to measure 17-hydroxyprogesterone and Delta4-androstenedione in serum. *Mol Cell Endocrinol*. 2017;450:105-112.
27. Bouxsein ML, Boyd SK, Christiansen BA, Guldberg RE, Jepsen KJ, Muller R. Guidelines for assessment of bone microstructure in rodents using micro-computed tomography. *J Bone Miner Res*. 2010;25(7):1468-1486.
28. van der Eerden BC, Hoenderop JG, de Vries TJ, *et al*. The epithelial Ca2+channel TRPV5 is essential for proper osteoclastic bone resorption. *Proc Natl Acad Sci U S A*. 2005;102(48):17507-17512.
29. Gruber HE. Adaptations of Goldner's Masson trichrome stain for the study of undecalcified plastic embedded bone. *Biotech Histochem*. 1992;67(1):30-34.
30. van As C, Koedam M, McLuskey A, *et al*. Supplementary data for: Loss of anti-Müllerian hormone signaling in mice affects trabecular bone mass in a sex- and age-dependent manner. *Figshare*. Deposited September 14, 2022. doi: 10.6084/m9.figshare.21103162
31. Wright LE, Christian PJ, Rivera Z, *et al*. Comparison of skeletal effects of ovariectomy versus chemically induced ovarian failure in mice. *J Bone Miner Res*. 2008;23(8):1296-1303.
32. Haas JR, Christian PJ, Hoyer PB. Effects of impending ovarian failure induced by 4-vinylcyclohexene diepoxide on fertility in C57BL/6 female mice. *Comp Med*. 2007;57(5):443-449.
33. Gaddy-Kurten D, Coker JK, Abe E, Jilka RL, Manolagas SC. Inhibin suppresses and activin stimulates osteoblastogenesis and osteoclastogenesis in murine bone marrow cultures. *Endocrinology*. 2002;143(1):74-83.
34. Perrien DS, Akel NS, Edwards PK, *et al*. Inhibin A is an endocrine stimulator of bone mass and strength. *Endocrinology*. 2007;148(4):1654-1665.
35. Wang Y, Newton H, Spaliviero JA, *et al*. Gonadotropin control of inhibin secretion and the relationship to follicle type and number in the hpg mouse. *Biol Reprod*. 2005;73(4):610-618.
36. Perrien DS, Achenbach SJ, Bledsoe SE, *et al*. Bone turnover across the menopause transition: correlations with inhibins and follicle-stimulating hormone. *J Clin Endocrinol Metab*. 2006;91(5):1848-1854.
37. Mills EG, Yang L, Nielsen MF, Kassem M, Dhillo WS, Comninos AN. The relationship between bone and reproductive hormones beyond estrogens and androgens. *Endocr Rev*. 2021;42(6):691-719.
38. Cimino I, Casoni F, Liu X, *et al*. Novel role for anti-Mullerian hormone in the regulation of GnRH neuron excitability and hormone secretion. *Nat Commun*. 2016;7(1):10055.
39. Santoro N. The menopausal transition. *Am J Med*. 2005;118(Suppl 12B):8-13.
40. Kim JH, Yang YR, Kwon K-S, Kim N. Anti-Mullerian hormone negatively regulates osteoclast differentiation by suppressing the receptor activator of nuclear factor-kappaB ligand pathway. *J Bone Metab*. 2021;28(3):223-230.
41. Griffith JF, Yeung DK, Ma HT, Leung JC, Kwok TC, Leung PC. Bone marrow fat content in the elderly: a reversal of sex difference seen in younger subjects. *J Magn Reson Imaging*. 2012;36(1):225-230.
42. Shen W, Chen J, Punyanitya M, Shapses S, Heshka S, Heymsfield SB. MRI-measured bone marrow adipose tissue is inversely related to DXA-measured bone mineral in Caucasian women. *Osteoporos Int*. 2007;18(5):641-647.
43. Morita Y, Iwamoto I, Mizuma N, *et al*. Precedence of the shift of body-fat distribution over the change in body composition after menopause. *J Obstet Gynaecol Res*. 2006;32(5):513-516.